ACADEMIC PRESS

Available online at www.sciencedirect.com
SCIENCE DIRECT®

Journal of Catalysis 217 (2003) 367–375

JOURNAL OF CATALYSIS

www.elsevier.com/locate/jcat

The role of suprafacial oxygen in some perovskites for the catalytic combustion of soot

Debora Fino,* Nunzio Russo, Guido Saracco, and Vito Specchia

Department of Materials Science and Chemical Engineering, Politecnico di Torino, Corso Duca degli Abruzzi 24, 10129 Torino, Italy

Received 31 October 2002; revised 19 February 2003; accepted 19 February 2003

Abstract

High specific-surface-area bulk perovskites (18–25 m^2/g) have been synthesized by the *combustion synthesis* method as catalysts for the combustion of soot, a major pollutant emitted by diesel engines. The activity order for soot combustion was found to be $LaCrO_3 > LaFeO_3 > LaMnO_3$, which is just the reverse of the intrinsic activity toward methane combustion, another major application field for perovskites. On the grounds of a characterization based on XRD, SEM, TEM, TPD, and TPR analyses as well as on reactive runs, the prevalent activity of the chromite catalyst could be explained by its higher concentration of suprafacial, weakly chemisorbed oxygen, which contributes actively to soot combustion by *spillover* in the temperature range 300–500 °C, but negligibly to methane combustion. The best catalyst prepared ($La_{0.9}K_{0.1}Cr_{0.9}O_{3-\delta}$) could ignite soot combustion well below 400 °C, which is inside the range of temperatures reached at the exhaust line of a diesel engine. Maximization of the concentration of suprafacial oxygen is pointed out as the main pathway to follow for the development of new, more active catalysts.

Keywords: $La_{0.9}K_{0.1}Cr_{0.9}O_{3-\delta}$; Perovskite-type chromites; Catalytic combustion; Diesel particulate; Soot; Suprafacial oxygen

1. Introduction

Diesel engines power most of the trucks, buses, trains, ships, and off-road machinery such as construction and agricultural equipment. With mounting evidence that diesel exhaust poses major health hazards, the reduction of diesel pollution has become a public priority. Diesel engines emit large quantities of particulate matter (called PM) and nitrogen oxides (NO_x), both precursors of photochemical smog [1]. Particulate irritates the eyes and nose and aggravates respiratory problems. It has also been directly associated with an increased risk of premature death by cancer. Researchers estimate that tens of thousands of people die each year as a result of particulate pollution [2]. The International Agency for Research on Cancer classifies diesel exhaust as a probable human carcinogen, and the US Environmental Protection Agency has proposed the same classification [3,4]. Especially dangerous for human health are particles less than 2.5 μm in size. Starting from January 2000 the highest level admitted for Diesel particulate emissions was 0.04 g/km. Even more severe limits have been fixed for the year 2005 (0.025 g/km).

Diesel particulate filters (DPF) are generally recognized as the most viable solution to the problem [5]. The filter durability is closely entailed by the successful control of periodic regeneration by combustion of the deposited particulate. Frequent regeneration prevents undesired backpressure buildup related to the particulate accumulated in the filter. Since the temperature of the exhaust gases of modern diesel engines is relatively low (150–400 °C), well below the ignition temperature of diesel particulate in air (550–600 °C), the oxidation reaction should be supported by a catalyst deposited onto the trap.

The last-generation Common Rail diesel engines enable the occasional postinjection of some fuel that gets burned in a specific honeycomb oxidation catalyst placed upstream of the trap. The consequent temperature rise of the exhaust gases help ignite the catalytic combustion of the soot trapped, eventually leading to trap regeneration [6].

Any catalyst to be placed over the trap should possess high thermochemical stability and intrinsic activity, to ignite reliably the soot as early as possible, thereby limiting the amount of postinjected fuel (a net loss from the economi-

* Corresponding author.
E-mail address: debora.fino@polito.it.

0021-9517/03/$ – see front matter
doi:10.1016/S0021-9517(03)00143-X

cal view point). In this context, large varieties of catalytic materials for diesel soot abatement are being developed and evaluated [7–10]. Our current research efforts are aimed at the development of catalytic systems based on perovskite oxides ($A_{1-x}A'_xB_{1-y}B'_yO_{3\pm\delta}$, where A, A′ = La or K and B, B′ = Mn, Cr, and Fe), because of their good stability and intrinsic catalytic activity.

The work here presented concerns the synthesis, characterization, catalytic activity test, and reaction mechanism assessment of a series of La–Cr perovskites, whose performance is compared with that of other perovskites (i.e., $LaMnO_3$ and $LaFeO_3$). Some conclusions are then drawn concerning either the role of each single constituting element on the activity of the most promising catalyst ($La_{0.9}K_{0.1}Cr_{0.9}O_{3-\delta}$), or its reaction mechanism and kinetics pointing out the way to the development of new, more active catalysts.

2. Experimental

2.1. Catalyst preparation

A series of perovskite samples ($LaMnO_3$, $LaFeO_3$, $LaCrO_3$, $LaCr_{0.9}O_{3-\delta}$, and $La_{0.9}K_{0.1}Cr_{0.9}O_{3-\delta}$) were prepared via a highly exothermic and self-sustaining reaction, the so-called "*combustion synthesis*" method [11,12]. This technique is particularly suited to produce nanosized particles of catalyst. A nanostructured catalyst coating over the trap could effectively improve the local catalyst-soot contact conditions, a critical issue in this field as discussed in the introduction.

The synthesis process can be formally split into two steps (the preparation of lanthanum manganate is here considered as an example)

$$La(NO_3)_3 + Mn(NO_3)_2 \rightarrow LaMnO_3 + \tfrac{5}{2}N_2 + 6O_2, \quad (1)$$

$$4CO(NH_2)_2 + 6O_2 \rightarrow 4CO_2 + 8H_2O + 4N_2. \quad (2)$$

The first one is endothermic and represents the real perovskite synthesis starting from the metal nitrate precursors (1), while the second is exothermic and accounts for the reaction between oxygen derived from nitrates decomposition and urea (2). Some direct combustion of urea with atmospheric oxygen cannot of course be excluded as the preparation is carried out in air within an electric oven kept at 500 °C hosting the precursors mixture placed in a porcelain vessel (see [12] for more details).

The overall set of reactions is markedly exothermic, which leads within the reacting solid mixture to a thermal peak well exceeding 1000 °C for a few seconds. To emphasize this sudden heat release, some NH_4NO_3 was added on purpose to the precursor mixture, as indicated in [12]. Under these conditions nucleation of perovskite crystals is induced, their growth is limited, and nanosized grains can be obtained, as earlier anticipated.

After preparation, all catalysts were ground in a ball mill at room temperature and submitted to physical and chemical characterization.

2.2. Catalyst characterization

X-ray diffraction (PW1710 Philips diffractometer equipped with a monochromator for the Cu-K_α radiation) was used on all fresh catalyst to examine whether the desired perovskite structure was actually achieved.

The BET specific surface areas of the prepared catalysts were evaluated from the linear parts of the BET plot of the N_2 isotherms, using a Micromeritics ASAP 2010 analyzer. For bulk and nonporous catalysts as perovskite ones the specific surface area can be directly related to the average crystal size. However, direct observation was also performed by transmission electron microscopy (TEM, Philips CM 30 T), employed to analyze in more detail the microstructure of the different catalyst powders.

Scanning electron microscopy (SEM) and energy dispersion spectroscopy (EDS) (Philips, Model 515 SEM equipped with EDAX PV9900 EDS) were used to investigate the morphology as well as the elemental composition and distribution of all the catalyst. Compositional analysis (dissolution in HNO_3/HCl followed by atomic absorption analysis with a Perkin-Elmer 1100B spectrometer), performed an all prepared samples, confirmed that the overall amount of the various elements of interest (La, K, Cr, Mn, Fe, O) was consistent with that used in the precursors and was compatible with the phases detected by X-ray diffraction with a ±4% deviation.

2.3. Catalytic activity tests

The catalytic activity of the prepared catalysts was tested in a temperature-programmed combustion (TPC) apparatus. A detailed description of the TPC equipment has been reported in a previous paper of ours [13]. This equipment mainly consists of a fixed bed inserted in a quartz microreactor (i.d.: 4 mm). The fixed bed was prepared by mixing 50 mg of a 1:9 by weight mixture of carbon and powdered catalyst with 150 mg of silica pellets (0.3–0.7 mm in size); this inert material was adopted to reduce the specific pressure drops across the reactor and to prevent thermal runaway. Amorphous carbon particles by Cabot Ltd. of about 45 nm in diameter, with BET specific surface area of 200 m^2/g, with 0.34% of ashes after calcination at 800 °C and 12.2wt% of adsorbed water moisture, without adsorbed hydrocarbons and sulfates, were used for the sample preparation. Amorphous carbon was used for such investigations because it burns at temperatures close to those characteristic of diesel particulates. The catalyst/carbon/SiO_2 mixture was inserted in the reactor and confined between two layers of quartz wool. The reactor was placed in a PID-regulated oven and a K-type thermocouple was inserted in the packed bed. The tests were carried out by heating the sample up to 700 °C

(heating rate 5 °C/min) with a mass flow meter delivering an air flow toward the microreactor (100 ml/min). The carbon conversion was monitored with a NDIR analyzer (Hartman and Braun URAS 10E) measuring the carbon dioxide concentration in the reactor outlet gases. A computer records both the fixed bed temperature and the CO_2 outlet concentration as a function of time. The CO_2 outlet concentration increases starting from the carbon ignition temperature, reaches a maximum, and then decreases as a consequence of carbon consumption. The temperature corresponding to the CO_2 peak (T_p) can be taken as an index of the activity of each tested catalyst. The lower the T_p value, the more active the catalyst. The runs were in any case repeated three times and the average T_p value was assumed for each catalyst. The maximum deviation between the T_p values derived in twin runs never exceeded 20 °C. Moreover, some balance point measurements on a diesel engine apparatus to evaluate the stability of the catalysts over 5 operating hours were performed in a previous paper of ours [14]. These studies confirmed that the activity of these materials remain almost unaffected under practical operating conditions.

Some comparative tests were also performed on all the prepared catalysts to check their activity toward methane combustion in the same apparatus described above and according to the procedures, carefully described in [13]. After a 30-min stay in air flow as a common pretreatment, a gas flow rate (1.2 cm^3/s of the following composition: $CH_4 = 1.5\%$, $O_2 = 18\%$, He = balance) was fed to a fixed bed of 1 g of catalyst particles (obtained by pressing the perovskite powders into tablets and then crushing into 0.2 ± 0.5-mm granules). The fixed bed was enclosed in a quartz tube (internal diameter: 4 mm) and sandwiched between two quartz wool layers. The reactor temperature was then lowered at a 38 °C/min rate down to 300 °C, meanwhile methane conversion was monitored by analyzing the outlet concentration of CO_2 (the only carbon oxidation product) by use of the same NDIR analyzer introduced above. From typical sigma-shaped curves obtained, methane half-conversion temperatures (T_{50}) were estimated as an index of catalytic activity toward methane combustion. As for soot combustion, each data point was obtained as the average of three twin runs performed on different samples of the same material. The deviation between the conversion measured at the same temperature in such runs was always less than 15 °C.

In order to fully appreciate the catalytic effect of the perovskites, blank runs in the absence of the catalyst and just in the presence of the inert SiO_2 were carried out for both soot and methane combustion cases.

2.4. Activation energy assessment by the Ozawa method

The activation energy of soot combustion over the prepared catalysts was measured according the Ozawa method described below on the grounds of DSC runs carried out in a Perkin–Elmer DSC-Pyris equipment. Ten milligrams of a 9/1 by weight catalyst/carbon mixture was analyzed (the same weight of alumina as a reference) during a temperature scan from 50 to 720 °C (heating rates 5, 10, 20, 30, and 50 °C/min). An air flow (100 ml/min) provided the oxygen required for carbon combustion. DSC patterns were processed, thus obtaining the onset and the maximum temperatures of the exothermic combustion peak. The temperatures corresponding to the cumulative combustion of both 25 and 50 wt% of the total carbon put in the sample holder were also calculated on the grounds of simple calculations. DSC scans were also performed (in the experimental conditions reported above) on an alumina/carbon mixture, so as to estimate the activation energy of the noncatalyzed combustion of carbon.

The activation energy can be evaluated through the so-called Ozawa procedure [15,16] by proper interpretation of thermal analysis data. According to this method, the following relationship links the values of the heating rate with the corresponding values of temperature (T_α) at which a fixed fraction α of carbon is burned during each run

$$\ln \Phi = B - 0.4567\left(\frac{E_a}{R \cdot T_\alpha}\right),$$

where B is a constant lumping α-dependent terms. If the heat released by the combustion is assumed to be proportional to the fraction α of converted carbon, once a reference α value (e.g., 50%) is closen, the T_α value corresponding to such value can be easily derived from the DSC curves by evaluating, via a simple integration, the amount of heat released by combustion. By least-square fitting of the $\ln \Phi$-vs-$1/T_\alpha$ data series, estimates of the activation energy can be obtained from the slope of the best-fitting line.

2.5. TPD–TPR analysis

Some further analyzes were performed on all the prepared perovskites in a Termoquest TPD/R/O 1100 analyzer, equipped with a thermal conductibility (TCD) detector. A fixed bed of catalyst was enclosed in a quartz tube and sandwiched between two quartz wool layers; prior to each temperature-programmed desorption (TPD) run, the catalyst was heated under an O_2 flow (40 ml/min) up to 750 °C. After a 30-min stay in O_2 flow at this temperature as a common pretreatment, the reactor temperature was then lowered down to room temperature by keeping the same flow rate of oxygen, thereby allowing complete oxygen adsorption over the catalyst. Afterward, helium was fed to the reactor at 10 ml/min flow rate and kept for 1 h at room temperature in order to purge out any excess oxygen molecule. The catalyst was then heated to 1100 °C at a constant heating rate of 10 °C/min using helium under a flow rate of 10 ml/min of helium. The O_2 desorbed during the heating was detected by the TCD detector.

Temperature-programmed reduction (TPR) experiments were then carried out in the same apparatus. After the same pretreatment adopted for the TPD runs, the sample was reduced with a 4.95% H_2/Ar mixture (10 ml/min) meanwhile

heating 10 °C/min up to 1100 °C. Once again via the TCD detector the amount of the H_2 reacted away could be monitored.

X-ray diffraction was employed on the catalysts which underwent each TPD or TPR analysis, to check whether the perovskite structure had been retained or not, and to detect the possible appearance of new phases.

2.6. Compatibility with wall-flow trap materials

Two different ceramic supports have been selected in order to evaluate the stability and the eventual reactivity between the perovskite catalysts and the ceramic support: a cordierite ($2MgO \cdot 2Al_2O_3 \cdot 5SiO_2$) filter produced by CORNING and a silicon carbide (SiC) filter industrialized by Ibiden (for both monoliths: cell structure = 14/200–300, diameter = 30 mm, length = 6–12 inch; pore diameter of channel walls = 9 μm, porosity of channel walls = 42%). Powders of both wall-flow materials were obtained from trap samples by crushing and ball milling. Such powders were then mixed with the most promising catalyst, $La_{0.9}K_{0.1}Cr_{0.9}O_{3-\delta}$ (weight ratio of 1:1), and kept for 24 h at 900 °C in air. The mixed powders were then characterized by XRD analysis in order to investigate the possible formation of new crystalline species by chemical reaction with the catalyst. Finally, this ceramic material-catalyst mixture was added to carbon to obtain samples for TPC analysis and assess the change of catalytic activity that eventually occurred.

3. Results and discussion

All perovskite samples were found to be well crystallized by XRD analysis. No secondary phases could be detected by this technique (X-ray diffraction has a ±4% precision). Fig. 1 illustrates the diffraction spectrum recorded for the most important perovskite synthesized for this study, the $La_{0.9}K_{0.1}Cr_{0.9}O_{3-\delta}$ catalyst: it confirms the presence of a perfectly pure and crystalline phase. Fig. 2 shows SEM pictures of $LaMnO_3$ perovskite catalyst produced via combustion synthesis. Its microstructure appears foamy. During combustion synthesis, the decomposition/combustion of reacting precursors generates a large amount of gaseous products in a very short period of time, which leads to a spongy catalyst morphology. This feature represents a great advantage, as it favors the formation of rough interfaces for the catalyst powder agglomerates, which in turn intensify the contact conditions between the catalyst and the soot that accumulates over them. In the present context, perovskite crystals having a size of the same order of magnitude as that of the particulate are expected to provide the highest specific number of contact points between the soot directly captured over the catalyst layer and the crystals constituting such a layer. The TEM pictures in Fig. 3, and the one in Fig. 3b in particular, show that most of the perovskite crystals have a size ranging between 10 and 20 nm, which satisfies the above requirement. Moreover, this particle size is perfectly in line with the later-discussed BET surface areas of the various prepared catalysts (15–25 m^2/g). Once assumed that the average density of the catalyst particles equals to 6500 kg/m^3 [17], an average value for the perovskites tested, and a spherical shape for the particles themselves, it can be easily calculated that the above range size should correspond approximately to specific surface areas in the range 23–46 m^2/g. This slight discrepancy could be ascribed to the fact that perovskite crystals are not spherical (Fig. 3b).

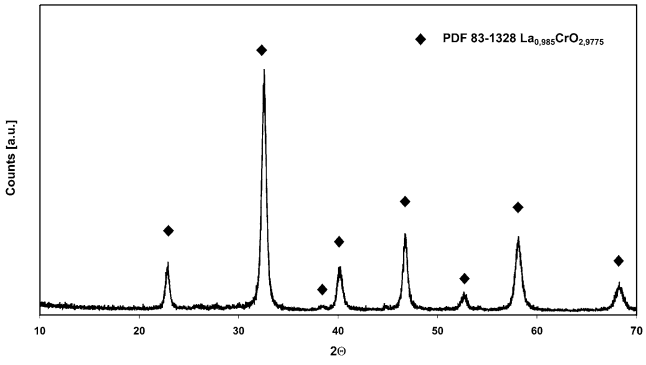

Fig. 1. XRD diffraction pattern of the $La_{0.9}K_{0.1}Cr_{0.9}O_{3-\delta}$ catalyst; markers are located according to the PDF 83-1328 $La_{0.985}CrO_{2.9775}$ card.

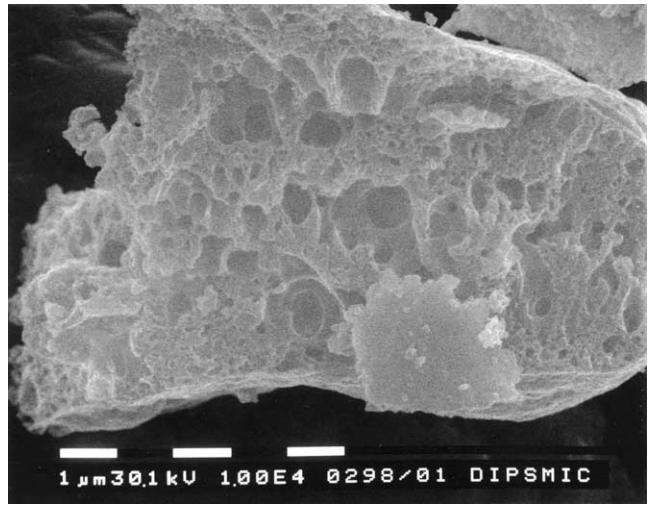

Fig. 2. SEM microstructure $LaMnO_3$ (calcination temperature, 600 °C; 10,000×).

Fig. 4 summarizes the methane half conversion temperatures, the carbon combustion peak temperatures, the BET specific surface area, and the activation energies of all the perovskite catalysts investigated.

In line with literature information [18–20] the following activity order for methane combustion is followed between the perovskites containing Mn, Fe, and Cr: $LaMnO_3 > LaFeO_3 > LaCrO_3$. The use of substoichiometric chromium amount seems to improve slightly the catalytic activity, despite the very moderate loss of specific surface area (SSA)

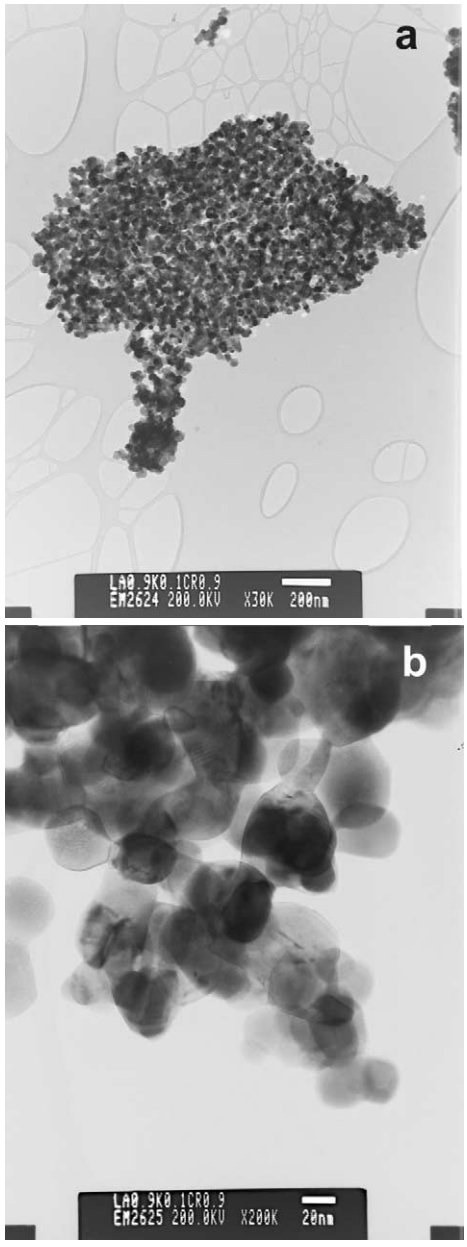

Fig. 3. TEM micrographs of the $La_{0.9}K_{0.1}Cr_{0.9}O_{3-\delta}$ catalyst crystals. (a) Overall view (30,000×); (b) particular (200,000×).

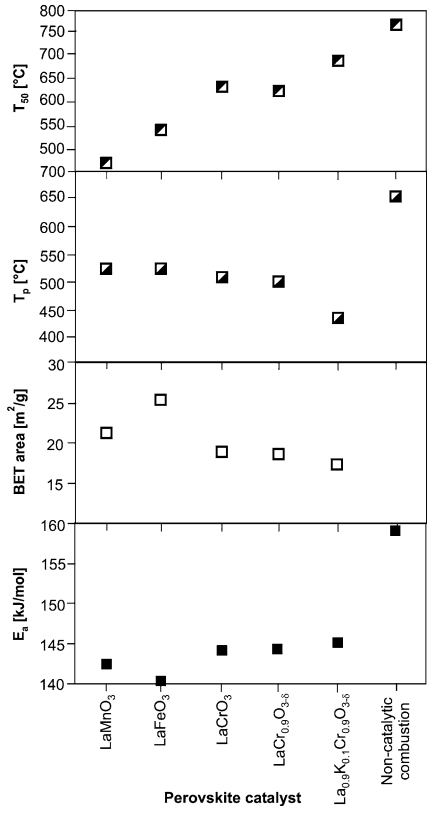

Fig. 4. Results of the screening tests on the activity T_{50}, half-conversion temperature of methane, and T_p, peak temperature of CO_2 production during soot combustion), BET specific surface area and activation energy of the various perovskite catalysts developed. Data concerning the noncatalytic carbon combustion are also shown for a comparison.

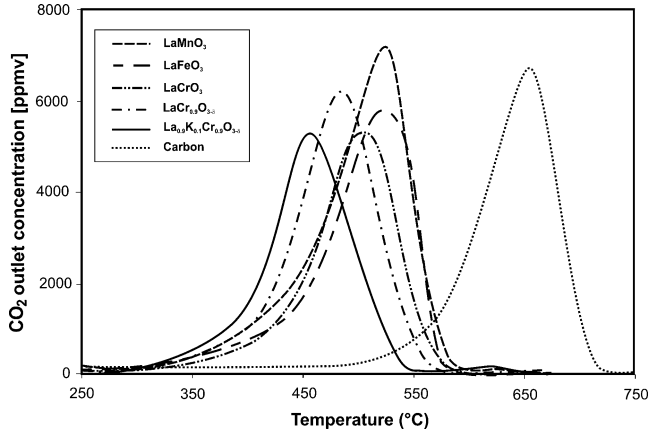

Fig. 5. TPC runs performed with all selected perovskite catalysts; that of the noncatalytic carbon combustion is also drawn for a comparison.

measured when shifting from $LaCrO_3$ to $LaCr_{0.9}O_{3-\delta}$. Partial substitution of lanthanum with potassium seems to reduce the catalytic activity. Such a loss is more pronounced than the parallel loss of SSA registered. As a consequence such lower activity might not only be due to loss of active sites but to a change in the reactivity of the oxygen chemisorbed on the perovskite surface oxygen. All catalysts guarantee much lower T_{50} values than the one related to noncatalytic combustion (780 °C).

Shifting the soot combustion, the key application pursued in the present paper, according to the data plotted in Figs. 4 and 5, the catalysts show TPC peak temperatures significantly lower than 650 °C (noncatalytic combustion). The superior activities of $LaCr_{0.9}O_{3-\delta}$ and $La_{0.9}K_{0.1}Cr_{0.9}O_{3-\delta}$ perovskites can clearly be seen. $La_{0.9}K_{0.1}Cr_{0.9}O_{3-\delta}$ in particular shows a CO_2 peak temperature (T_p) at only 455 °C. Nevertheless, it is surprising how the catalysts belonging to the chromite class are more active than $LaMnO_3$ and $LaFeO_3$ catalysts, which, as emphasized above were found to be much better catalysts for the combustion of methane [18–20].

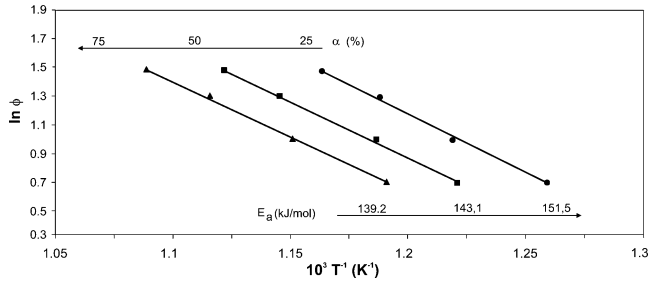

Fig. 6. Ozawa plots of the $LaCrO_3$ catalyst for the determination of the activation energy (E_a) at different levels of carbon conversion (α).

The values of activation energy for carbon combustion, calculated for the various prepared perovskites via the Ozawa method (see typical Ozawa plots in Fig. 6), are not very different from one another, which seems to entail that the different perovskites are capable of delivering oxygen species of similar nature to the reacting carbon particulate. The same type of reaction oxygen species should in fact lower the activation energy of noncatalytic soot combustion to a constant extent for all perovskites.

If the SSA values reported in Fig. 4 are now considered, it is worth noting that perovskites with quite high values of specific surface area can be obtained (compared to a lower specific surface area achievable by the "citrates" method; i.e. a few m^2/g [18,19]). Unfortunately, the value related to chromite is lower than those of the manganate and the ferrite perovskites, which does not help to explain the superior soot combustion activity of chromites and of the $La_{0.9}K_{0.1}Cr_{0.9}O_{3-\delta}$ pervoskite in particular, compared to their counterparts. The main reason for the superior activity of chromites should thus lie in a significantly higher specific surface concentration of active oxygen species compared to that of the ferrite or the manganate. As declared earlier, transient studies (TPD/TPR) were carried out to better elucidate this point.

It is well known that, when a perovskite is heated at high temperature, oxygen vacancies can be formed. As thoroughly discussed in a review by Seyama [20] and reported in a number of papers (e.g., [21–27]), two types of chemisorbed oxygen species are noted accompanied by related desorption peaks: a low-temperature species, named hereafter α, desorbed in the 300–600 °C range, and a high-temperature one, named β in the following, desorbed at 600–900 °C. The α peak is not always observable and strongly depends on the concentration of surface oxygen vacancies. In particular its onset and intensity depend in part on the nature of the metal B of the ABO_3 structure, but mainly on the degree of substitution of the A ion with ions of lower valence [22]. The β peak, characterized by a higher onset temperature, is strictly related to the nature of the B ion and its occurrence is strictly linked to redox transitions of the valence state of this ion. When the A ion is partially substituted with an ion of different oxidation state (as for the $La_{0.9}K_{0.1}Cr_{0.9}O_{3-\delta}$ catalyst) a charge compensation is required so as to achieve electroneutrality. This can either be achieved by formation of oxygen vacancies of by shift of the B metal toward higher valences (e.g., $Cr^{3+} \rightarrow Cr^{4+}$). According to the above literature information, this substitution might actually result in an increase of both α and β types of oxygen.

The presence of Cr^{4+} was demonstrated to promote an increase of catalytic activity toward methane combustion [18]. The most likely explanation is that the perovskite can act as an oxygen pump toward the methane molecule. Oxygen can indeed be made available to the combustion in combination with a temporary shift of Cr valence from 4+ back to 3+. Oxygen molecules coming from the gaseous atmosphere can reoxidize the perovskite and set back Cr^{4+} species. Such an intrafacial mechanism was first proposed by Voorhoeve et al. [28] and should mostly regard β-type oxygen species.

The TPD results shown in Fig. 7a seem thus to suggest that α-type oxygen and not β-type should be responsible for the superior activity of chromites toward soot combustion.

If attention is focused on the temperature range 400–500 °C, where the most active perovskite tested displayed their best soot combustion activities (see the CO_2 peaks in Fig. 5), Fig. 7a shows that only chromite-based perovskites display significant oxygen desorption in this temperature range. Such α-type weakly chemisorbed "suprafacial" species should likely be those responsible for soot combustion. It is perhaps possible that these α-type oxygen could undergo *spillover* [6] over the carbon agglomerates in touch

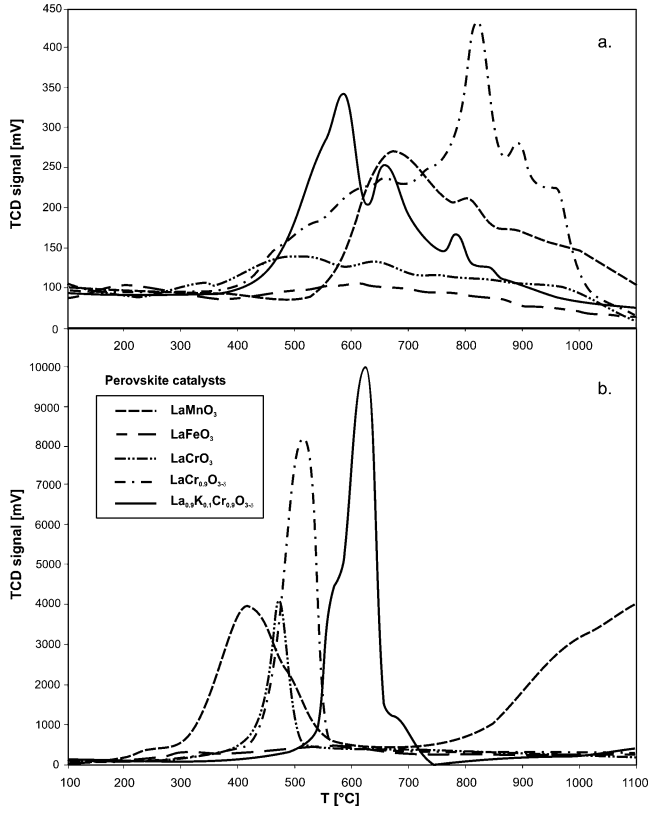

Fig. 7. Results of the temperature-programmed desorption (a) and reduction (b) tests on all selected perovskite catalysts; low-temperature oxygen species α; high-temperature oxygen species β.

with the catalyst. This would result in an increase of the number of sites in which the carbon particles are simultaneously attacked by the oxygen, to the benefit of reaction kinetics.

The higher surface concentration of α-type oxygen should also explain why, despite a similar activation energy and an even lower BET surface area, chromite perovskites do burn out soot at temperatures lower than lanthanum manganate. This last perovskite shows indeed negligible oxygen desorption unless temperatures are higher than 550 °C. The β-type oxygen desorbed at such high temperatures is actually associated to intrafacial species, less easy to desorb by thermal means [29–32]. In earlier studies of ours [19], it was demonstrated how this β-type oxygen could be responsible for ignition of natural gas combustion, through an Elay–Rideal mechanism. Such a mechanism leads, as a first step, to hydrogen abstraction from the methane molecule by reaction with monoatomic intrafacial oxygen. Such a reaction step, quite accelerated by lanthanum manganate, seems to be of minor importance for soot combustion for which suprafacial oxygen, present in large amounts on chromite-type perovskites, seems to be the key player.

In line with the literature data [33], it must be stressed that chromite catalysts do lose intrafacial oxygen at high temperatures. A number of desorption peaks can be noted at temperatures higher than 600 °C, possibly associated with different β-type oxygen species more and more bound to the perovskite structure and therefore less and less easy to desorb. The precise determination of the nature of such oxygen species goes beyond the scopes of the present paper, especially because these species should not play a significant role in carbon combustion for the reasons stated above.

As a final consideration, lanthanum ferrite seems to display very limited oxygen desorption both in the α and in the β-oxygen temperature regions, which confirms the earlier observations of other authors [34,35]. This is directly related to its average activity either for methane (Fig. 3 and [36]) or for soot combustion.

As stated earlier, some further TPR runs were performed to possibly get further information about the reaction mechanism. The results of such investigations are reported in Fig. 7b. The most impressive result concerns lanthanum manganate. The presence of hydrogen seems indeed to anticipate by nearly 300 °C the loss of β-type oxygen compared to the TPD case. This is in line with the peculiar attitude of $LaMnO_3$ to burn out hydrocarbons (see Fig. 4 and [20]), for which, as pointed out earlier, hydrogen abstraction is the first, kinetics-controlling step. It can further be noted that an hydrogen atmosphere can even lead to destruction of this perovskite material already at 900 °C, which was indicated by the second large reduction peak observed in Fig. 7b and actually verified by X-ray diffraction analysis (see also [29, 30,32]).

As far as chromite catalysts are concerned, the presence of hydrogen also anticipates the loss of β-type oxygen compared to the TPD case, but to a lower extent than

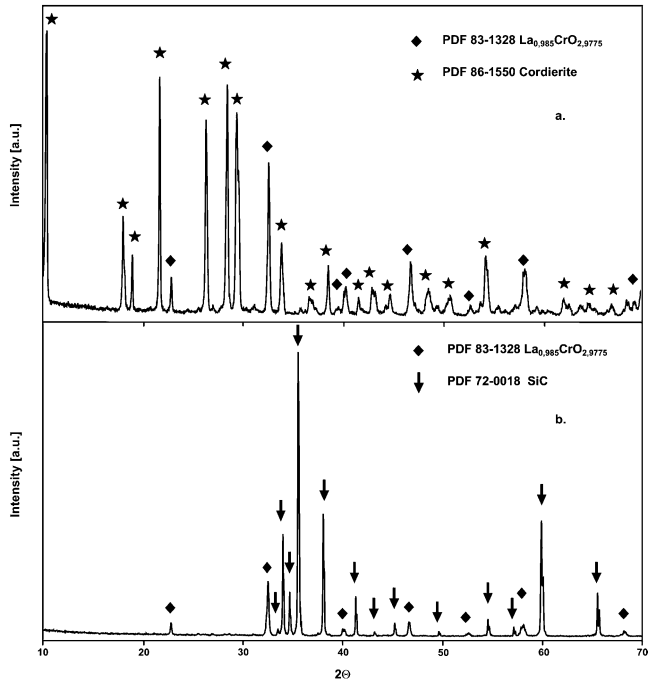

Fig. 8. XRD diffraction pattern of the $La_{0.9}K_{0.1}Cr_{0.9}O_{3-\delta}$ catalyst (according to the PDF 83-1328 $La_{0.985}CrO_{2.9775}$ card) and (a) cordierite (according to the PDF 86-1550 card) and (b) SiC (according to the PDF 72-0018 card) wall-flow support powder (weight ratio of 1:1) and calcinated for 24 h at 900 °C.

for $LaMnO_3$. This anticipation leads to a very sharp and intensive reduction peak, likely lumping, at least for the unsubstituted chromites, both α- and β-species. It can be seen how the area of this peak is significantly wider for the substoichiometric chromite, which explains its higher activity toward methane combustion than $LaCrO_3$.

As for the $La_{0.9}K_{0.1}Cr_{0.9}O_{3-\delta}$ catalyst, it could be reasoned that the presence of K stabilizes the Cr^{4+} species and renders its bonding to β-type oxygen stronger than for the other chromites. Hence, the TPR peak of this species appears to be shifted to higher temperatures. It can be reasoned that this is the main reason why this perovskite shows the lowest catalytic activity toward methane combustion among those of the catalysts tested. This feature does not seem to have any role in the combustion of soot for which α-type oxygen should play a prevalent role. It must be underlined that at typical methane combustion temperatures (ca. 900 K) $La_{0.9}K_{0.1}Cr_{0.9}O_{3-\delta}$ may become partially reduced in the CH_4/O_2 stream. As a result Cr^{3+} ions might be formed both at the surface and in the bulk of the perovskite. In such a case, the formation of secondary phases (e.g., La_2O_3 or K_2O) cannot be excluded in the long term.

Finally, Fig. 7b shows how, once again, even in the presence of oxygen, the $LaFeO_3$ phase undergoes rather limited reduction.

Some final considerations should be made concerning the catalysts compatibility with the constituting materials of the traps. A good chemical compatibility between catalysts and ceramic materials (see Fig. 8) was in fact assessed by means

of XRD analysis after a suitable thermal treatment which shows that both SiC and cordierite supports and catalysts do not react together even at high temperatures (900 °C). Furthermore, the thermal treatment just results in a slight perovskite crystal growth (sharper and more intense diffraction peaks). This result was actually confirmed by means of TPC runs showing that no significant loss of catalytic activity had occurred during aging. This feature is a necessary prerequisite for the preparation of reliable catalytic traps based on the most promising catalyst developed ($La_{0.9}K_{0.1}Cr_{0.9}O_{3-\delta}$) over the mentioned trap for bench testing purposes.

4. Conclusions

Chromite catalysts were prepared by combustion synthesis, characterized and tested as catalysts for soot combustion. A comparative analysis of such catalyst with other Mn- and Fe-based perovskites showed that despite the activation energy values related to all the catalysts selected are quite similar, chromites display the best catalytic activity toward soot combustion. This was explained with the capability of these materials of delivering α-type, weakly chemisorbed oxygen species to the combustion process.

Regardless of its low specific surface area, the K-substituted chromite catalyst ($La_{0.9}K_{0.1}Cr_{0.9}O_{3-\delta}$) exhibits the highest activity as a consequence of its superior chemisorbed α-oxygen amount. Such a circumstance points the ways toward future catalyst developments. Materials characterized by the highest possible α-oxygen-type concentration seem to be the way to go, paying attention to their compatibility with either the trap constituting material or the poisoning components present in the diesel exhaust gas (e.g., sulphur). In this context, Ni-containing perovskites, despite their exceptionally high α-oxygen concentration [25,33], cannot be considered as suitable candidates since they could hardly withstand even a few ppm of SO_2. Studies are in progress along the pathway pointed out with a systematic study based on combinatorial catalysis.

Symbols

B	constant in the Ozawa method
E_a	activation energy (kJ mol^{-1})
$f(\alpha)$	whatever function of α
R	ideal gas constant = 8.314 J/(mol K)
t	time (s)
T	absolute temperature (K)
T_α	temperature at which a given α value is reached (K)
T_p	peak temperature of CO_2 production during soot combustion (K)
T_{50}	half-conversion temperature of methane (K)

Greek letters

α	fraction of converted soot
δ	oxygen excess/defect with respect to stoichiometric amount
Φ	heating rate (K s^{-1})

Acknowledgment

Financial support of the European Community (Project ART-DEXA, Advanced Regeneration Technologies for Diesel Exhaust Particulate Aftertreatment) is gratefully acknowledged.

References

[1] M.C. White, R.A. Etzel, W.D. Wilcox, C. Lloyd, Environ. Res. 65 (1994) 56.
[2] D.W. Dockery, C.W. Pope, New Engl. J. Med. 329 (1993) 1753.
[3] R. Bhatia, P. Lopipero, A.H. Smith, Epidemiology 9 (1998) 84.
[4] Environmental Protection Agency web site: http://www.epa.gov.
[5] R.M. Herck, S. Gulati, R.J. Farrauto, Chem. Eng. J. 82 (2001) 149.
[6] B.A.A.L. van Setten, M. Makkee, J.A. Moulijn, Catal. Rev. Sci. Eng. 43 (2001) 489.
[7] G. Saracco, C. Badini, N. Russo, V. Specchia, Appl. Catal. B 21 (1999) 233.
[8] C. Badini, G. Saracco, N. Russo, V. Specchia, Catal. Lett. 69 (2000) 207.
[9] M. Ambrogio, G. Saracco, V. Specchia, Chem. Eng. Sci. 56 (2001) 1613.
[10] D. Fino, G. Saracco, V. Specchia, Ind. Ceramics 22 (2002) 37.
[11] A.G. Merzahanov, J. Mater. Proc. Techn. 56 (1996) 222.
[12] A. Civera, M. Pavese, G. Saracco, V. Specchia, Catal. Today 2003, in press.
[13] D. Fino, G. Saracco, V. Specchia, Chem. Eng. Sci. 57 (2002) 4955.
[14] D. Fino, P. Fino, G. Saracco, V. Specchia, Chem. Eng. Sci. 58 (2003) 951.
[15] T. Ozawa, J. Therm. Anal. 2 (1970) 301.
[16] T. Ozawa, J. Therm. Anal. 7 (1975) 601.
[17] R.H. Perry, D.W. Green, J.O. Maloney, Perry's Chemical Engineers' Handbook, 6th ed., McGraw–Hill, New York, 1984.
[18] G. Saracco, G. Scibilia, A. Iannibello, G. Baldi, Appl. Catal. B 8 (1996) 229.
[19] G. Saracco, F. Geobaldo, G. Baldi, Appl. Catal. B 20 (1999) 277.
[20] T. Seyama, Catal. Rev. Sci. Eng. 34 (1992) 281.
[21] Y. Teraoka, M. Yoshimatsu, N. Yamazoe, T. Seyama, Chem. Lett. (1984) 893.
[22] N. Yamazoe, Y. Teraoka, Catal. Today 8 (1990) 175.
[23] M.S.G. Baythoun, F.R. Sale, J. Mater. Sci. 17 (1982) 2757.
[24] R. Lenza, I. Rossetti, L. Fabbrini, C. Oliva, L. Forni, Appl. Catal. B 28 (2000) 55.
[25] I. Rossetti, L. Forni, Catalytic, Appl. Catal. B 33 (2001) 345.
[26] L. Forni, I. Rossetti, Appl. Catal. B 38 (2002) 29.
[27] H.M. Zhang, Y. Shimizu, Y. Teraoka, N. Miura, N. Yamazoe, J. Catal. 121 (1990) 432.
[28] R.J.H. Voorhoeve, J.P. Remeika, D.W. Johnson, Science 180 (1973) 62.
[29] Y.Ng. Lee, R.M. Lago, J.L.G. Fierro, V. Cortes, F. Sapina, E. Martinez, Appl. Catal. A 207 (2001) 17.

[30] Y.Ng. Lee, R.M. Lago, J.L.G. Fierro, V. Cortes, J. Gonzalez, Catal. A 215 (2001) 277.
[31] P. Ciambelli, S. Cimino, S. De Rossi, M. Faticanti, L. Lisi, G. Minelli, I. Petitti, P. Porta, G. Russo, M. Turco, Appl. Catal. B 24 (2000) 243.
[32] S. Ponce, M.A. Pena, J.L.G. Fierro, Appl. Catal. B 24 (2000) 193.
[33] Y. Yokoi, H. Uchida, Catal. Today 42 (1998) 167.
[34] V.C. Belessi, A.K. Lavados, P.J. Pomonis, Appl. Catal. B 31 (2001) 183.
[35] V.C. Belessi, C.N. Costa, T.V. Bakas, T. Anastasiadou, P.J. Pomonis, A.M. Efstathiou, Catal. Today 59 (2000) 347.
[36] L.G. Tejuca, J.L.G. Fierro, in: Properties and Applications of Perovskite-Type Oxides, Dekker, New York, 1993.